

**A Kinetic Study for the Fenton and photo-Fenton Paracetamol Degradation in an Annular Photoreactor.**

Francesca Audino<sup>a</sup>, Leandro Oscar Conte<sup>b</sup>, Agustina Violeta Schenone<sup>b</sup>, Montserrat Pérez-Moya<sup>a</sup>, Moisès Graells<sup>a</sup>, and Orlando Mario Alfano<sup>b,\*</sup>

<sup>a</sup> Chemical Engineering Department, Universitat Politècnica de Catalunya, Escola d'Enginyeria de Barcelona Est (EEBE), Av. Eduard Maristany, 16, Barcelona 08019, Spain

<sup>b</sup> Instituto de Desarrollo Tecnológico para la Industria Química (INTEC), Consejo Nacional de Investigaciones Científicas y Técnicas (CONICET) and Universidad Nacional del Litoral (UNL), 3000 Santa Fe, Argentina

---

\* Corresponding author. Tel.: +54 342 451 1546 Ext. 1056. E-mail address: alfano@intec.unl.edu.ar (O. M. Alfano).

## **Abstract**

A kinetic model describing Fenton and photo-Fenton degradation of paracetamol (PCT) and consumption of hydrogen peroxide ( $\text{H}_2\text{O}_2$ ) was proposed. A set of Fenton and photo-Fenton experiments (18 runs in total) was performed by fixing the initial concentration of PCT to  $40 \text{ mg L}^{-1}$  and varying the initial concentrations of  $\text{H}_2\text{O}_2$  and ferrous ion,  $\text{Fe}^{2+}$ . The experimental set-up was a well-stirred annular photoreactor equipped with an Actinic BL TL-DK 36 W/10 1SL lamp. Experimental results highlighted that PCT is no more detected by HPLC analysis within a minimum reaction time of 2.5 and a maximum reaction time of 15.0 min. Besides, a maximum conversion of total organic carbon (TOC) of 68.5% was observed after 75 min of reaction in case of using UV radiation and the highest concentrations of the Fenton reagents. The experimental data were used to fit the kinetic model. The radiation field inside the reactor was taken into account through the Local Volumetric Rate of Photon Absorption, evaluated by assuming a line source model with spherical and isotropic emission. The kinetic parameters were estimated by using a non-linear least-squares regression procedure and Root Mean Square Errors (*RMSE*) were calculated in order to validate the feasibility of the proposed model. A good agreement between experimental and predicted data was observed and the lowest values of *RMSE* resulted in 5.84% and 9.59% for PCT and  $\text{H}_2\text{O}_2$  normalized concentrations, respectively.

**Keywords:** AOPs, pharmaceuticals, annular photoreactor, design of experiments, LVRPA, kinetic modelling

## 1 INTRODUCTION

In the last decades, a notable effort has been made to investigate the main aspects of the Advanced Oxidation Processes (AOPs). AOPs are a group of chemical processes all characterised by the capability of exploiting the high reactivity of  $HO\cdot$  radicals in driving oxidation reactions that are suitable for achieving pollutant remediation and mineralization (Andreozzi et al. 1999). Hence, AOPs represent a convenient application to wastewater treatment, also considering the possibility to combine the biological treatment with an oxidative degradation of toxic or refractory substances (Oller et al. 2011).

Especially, they can be adopted for the treatment of the so-called Contaminants of Emerging Concern (CECs). CECs are a group of chemicals, including pharmaceuticals and personal care products (PPCPs), which are increasingly being detected at low concentrations ( $ng\ L^{-1}$  to  $\mu g\ L^{-1}$ ) in surface water, ground waters and even drinking waters, and that may be included in future environmental regulations depending on the results of the investigations on their effects on the human health and environment (EPA). This shows that conventional sewage treatment plants are not able to remove this kind of contaminants.

According to the current legislation, the Directive 2013/39/EU of the European Parliament and of the Council of 12 August 2013 amending Directives 2000/60/EC and 2008/105/EC, an important factor to be taken into account is the CECs monitoring as well as the reinforcement of the risk assessment of pharmaceutical products (Ribeiro et al. 2015).

Regarding pharmaceuticals, in the last two decades, a large variety of drugs (analgesics, anti-inflammatory, antibiotics, etc.) coming from domestic, industrial, hospital and health centres waste waters or from landfill leachates, have been detected in soils, surface waters, ground waters and drinking waters.

Particularly, the photo-enhanced Fenton process has proved to be highly efficient in degrading CECs (Miralles-Cuevas et al. 2014) as well as strength organic wastewaters (Pouran et al. 2015). As a matter of fact, the review by Wang et al. (2016) highlighted several industrial applications of the photo-Fenton process that has been used to treat different kinds of wastewaters such as olive-oil mill, textile, pesticide, cosmetic, dye, fermentation brine, green olives, pharmaceutical, cork cooking, pulp mill and phenolic wastewaters.

The Fenton reaction is an old reactive system proposed by Fenton in 1894 (Fenton 1894), that occurs by means of addition of hydrogen peroxide ( $H_2O_2$ ) to ferrous ion salts ( $Fe^{2+}$ ) and that leads to the formation of hydroxyl radicals, mainly  $HO^\cdot$ . The photo-assisted Fenton process (Kiwi et al. 1993; Pulgarin et al. 1996) represents an extension of the Fenton process obtained by using a UV-VIS light source. Under irradiated conditions and acid medium (pH = 2.8), the photolysis of ferric ions ( $Fe^{+3}$ ) complexes ( $Fe(OH)^{2+}$ ) occurs, allowing the  $Fe^{+2}$  regeneration and the formation of an additional hydroxyl radical leading to a strong increase of the degradation rate of organic pollutants.

A large experimental effort has led to an extensive knowledge on photo-Fenton process. Several works, at both laboratory and pilot plant scale, have investigated the key process efficiency parameters, such as  $H_2O_2$  consumption, processing time and mineralization rate, as well as the effect of factors like temperature, pH, dissolved ion concentration and dissolved organic carbon (DOC) on such parameters (Andreozzi et al. 2000; Pignatello et al. 2006; Farias et al. 2007; Zapata et al. 2010). Conversely, despite the extensive experimental work, the mathematical modelling is still under development. Specifically, concerning photo-Fenton kinetics modelling, mainly three different approaches have been proposed: First Principles Models (FPMs), Empirical Models (EMs), and Data Based Models (DBMs). FPMs rely on the description of all the elementary steps of the process. The works by Kang et al. (2002), Jeyong et al. (2005), and Ortiz de la Plata et al. (2010), are representative examples of FPMs. On the other hand, EMs rely on a complete empirical approach based on the use of regression models (Kusic et al. 2006) eventually coupled with the design of experimental techniques (Pérez-Moya et al. 2008). Finally, in the area of DBMs, Artificial Neural Networks (ANN) (Göb et al. 2001), Support Vector Regression (SVR) (Shokry et al. 2015) and Ordinary Kriging (OK) (Shokry et al. 2015) have been used. While, currently, EMs and DBMs are unable to fully capture the complexity and nonlinear nature of such processes, the accuracy and understanding that might provide FPMs is unaffordable. Moreover, few works have addressed the modelling of the radiation field inside the photoreactor that requires the evaluation of the Local Volumetric Rate of Photon Absorption (LVRPA) (Cassano et al. 1995; Conte et al. 2016).

Thus, the present study aims at presenting a kinetic model that can be a compromise solution between the unaffordable complexity of the FPMs and the oversimplification of the EMs and DBMs, without disregarding the assessment of the LVRPA effect.

Paracetamol (*PCT*) was selected as model pollutant since it is one of the top 200 pharmaceuticals prescribed overall the world, being widely used as antipyretic and analgesic. Therefore, PCT is continuously released by hospital waste (Langford et al. 2009), as well as by consumer use and disposal (according to Muir et al. 1997, PCT is excreted in 58-68% during therapeutic treatment). As a consequence, it has been detected in the effluents of sewage treatment plants in  $\mu\text{g L}^{-1}$  (Ternes et al. 1998), in natural water sources at concentrations higher than  $65 \mu\text{g L}^{-1}$  in the Tyne River (UK) (Antunes et al. 2013) and even in groundwater at concentration ranging between  $\mu\text{g L}^{-1}$  and  $\text{ng L}^{-1}$  (De Gussemme et al., 2011).

However, another issue is the treatment of real paracetamol wastewaters that are characterized by high levels of PCT, Total Organic Carbon (TOC) and Chemical Oxygen Demand (COD) concentrations. A recent work by Dalgic et al. (2017) showed that the Fenton process can be an effective pre-treatment of a real paracetamol wastewater of the pharmaceutical industry characterized by a PCT concentration between 37 and  $294 \text{ mg L}^{-1}$ . Previously, Roshanfekar Rad et al. (2015) also investigated the use of photo-Fenton process in industrial applications. Particularly, these authors analysed the effect of different operational parameters on the photo-Fenton process including the phenol and paracetamol initial concentrations ranging between 20 and  $100 \text{ mg L}^{-1}$ . Cabrera Reina et al. (2012) proposed a model to track the photo-Fenton degradation of paracetamol present at high initial concentration ( $4\text{-}25 \text{ mmol L}^{-1}$  of TOC) or rather simulating an industrial wastewater.

In the present work, the experimental data set used to study the kinetic model was based on an initial concentration of PCT ( $[C_{PCT}^{t0}]$ ) of  $40 \text{ mg L}^{-1}$  (e.g. industrial wastewater). The initial  $\text{H}_2\text{O}_2$  concentration ( $[C_{\text{H}_2\text{O}_2}^{t0}]$ ) was varied between half and twice the stoichiometric dose to achieve mineralization of  $40 \text{ mg L}^{-1}$  of PCT and the initial ferrous ion concentrations ( $[C_{\text{Fe}^{2+}}^{t0}]$ ) between 5 and  $10 \text{ mg L}^{-1}$  (being the latter the maximum value allowed in wastewaters in Spain).

Reaction rates for PCT and  $\text{H}_2\text{O}_2$  were obtained and then ordinary differential equations (*ODEs*) were used for describing component mass balances inside the reactor. A line source radiation model with spherical and isotropic emission (*LSSE model*) was adopted in order to derive the equation describing the variation of LVRPA with the absorbing species.

Experimental and predicted concentrations of PCT and  $\text{H}_2\text{O}_2$  were compared by implementing a non-linear least-squares regression procedure in MATLAB and root mean square errors (*RMSE*) were calculated to test model reliability.

## **2 METHODOLOGICAL FRAMEWORK: EXPERIMENTAL SETTINGS AND PROCESS MODELLING**

The general methodology consists of an experimental part and a modelling section including model fitting (parameter estimation), that are detailed in the following sections.

### **2.1 EXPERIMENTAL**

The experimental step provides the data that will be used in the final optimisation procedure to estimate the kinetic constants of the proposed model.

#### **2.1.1 Reagent and chemicals**

Paracetamol 98% purity purchased from Sigma-Aldrich was used as model pollutant. Reagent-grade hydrogen peroxide 33% w/v from Panreac and iron sulfate ( $\text{FeSO}_4 \cdot 7\text{H}_2\text{O}$ ) from Merck adopted as the ferrous ion ( $\text{Fe}^{2+}$ ) source, were used to perform all the experiments. HPLC gradient grade methanol, MeOH, purchased from J.T. Baker and filtered milli Q grade water was used as HPLC mobile phases. High purity (>99%) ascorbic acid from Riedel de Haën, 0.2% 1,10-phenanthroline from Scharlab, sodium acetate anhydrous and 95%-98% sulfuric acid, both from Panreac, were used to perform iron species measurements. In order to adjust the initial pH to the optimal one ( $2.8 \pm 0.1$ ), hydrogen chloride HCl 37% from J.T. Baker was used. Distilled water was used as water matrix in all experiments.

#### **2.1.2 Analytical determinations**

Measurements of PCT, Total Organic Carbon (*TOC*),  $\text{H}_2\text{O}_2$ , and iron species concentrations were performed. *TOC* concentration ( $C_{\text{TOC}}$ ) was measured with a Shimadzu VCHS/CSN *TOC* analyser and samples were taken each 15 min until the end of the experiment. PCT concentration ( $C_{\text{PCT}}$ ) was determined using an HPLC Agilent 1200 series with UV-DAD. The measurement method is the one described by Yamal et al. (2014). All the samples, taken at 0, 1.5, 2.5, 5, 7.5, 10 and 15 min, were treated

with 0.1 M methanol (in proportion 50:50) to stop reaction and further degradation of PCT. Hydrogen peroxide concentration ( $C_{H_2O_2}$ ) was determined with a Hitachi U-2001 UV-VIS spectrophotometer and using the spectrophotometric technique described by Nogueira et al. (2005). This technique is based on the measurement of the absorption at 450 nm of the complex formed after reaction of  $H_2O_2$  with ammonium metavanadate. In this case, samples were taken each 5 min until a reaction time of 30 min and then each 15 min until the end of the assay.

The iron species ( $Fe^{2+}$ ,  $Fe^{TOT}$ ) were analysed using the 1,10-phenanthroline method following ISO 6332 (ISO 6332:1988), based on the absorbance measurements of the  $Fe^{2+}$ -phenanthroline complex at 510 nm. To measure total iron concentration ( $C_{Fe^{TOT}}$ ), ascorbic acid must be used so to convert all the ferric ions ( $Fe^{3+}$ ) to ferrous ions ( $Fe^{2+}$ ). Then, for difference, ferric ion concentration could be determined ( $C_{Fe^{3+}} = C_{Fe^{TOT}} - C_{Fe^{2+}}$ ). In this case, samples were taken each 5 min until a reaction time of 30 min and then each 15 min until the end of the assay.

Table 1 shows the experimental errors evaluated for all measurement techniques and for a PCT concentration range of  $[0-40] \text{ mg L}^{-1}$ , a Total Carbon (TC) concentration range of  $[0-50] \text{ mg L}^{-1}$ , an Inorganic Carbon (IC) concentration range of  $[0-10] \text{ mg L}^{-1}$ , and a  $H_2O_2$  concentration range of  $[0-150] \text{ mg L}^{-1}$ .

**Table 1.** Experimental errors of the measurement techniques

MEASUREMENT EQUIPMENT	MEASURED SPECIES	ERROR ( $\text{mg L}^{-1}$ )
HPLC Agilent 1200 series with UV-DAD	PCT	0.15
	$[0-40] \text{ mg L}^{-1}$	
Shimadzu VCHS/CSN TOC analyser	TC	0.23
	$[0-50] \text{ mg L}^{-1}$	
	IC	0.04
	$[0-10] \text{ mg L}^{-1}$	
Hitachi U-2001 UV-Vis spectrophotometer	$H_2O_2$	1.43
	$[0-150] \text{ mg L}^{-1}$	

### 2.1.3 Experimental set-up

A 15 L system composed by a 9-L glass jacketed reservoir tank and a 6-L glass annular photoreactor equipped with an Actinic BL TL-DK 36 W/10 1SL lamp (UVA-UVB) was used to perform Fenton and photo-Fenton experiments; the irradiated volume is 10% of the total volume (that is 1.5 L). The incident photon power,  $E = 3.36 \times 10^{-4}$  Einstein  $\text{min}^{-1}$  (300 and 420 nm) was measured by Yamal et al. 2014 using potassium ferrioxalate actinometry (Murov et al. 1993). In addition, the experimental device is also equipped with a pH sensor and a flowmeter for the control of the recirculation flow rate and a thermostatic bath for the temperature control, which is measured by a temperature sensor placed inside the 9-L tank. In Fig. 1, a schematic view (Fig. 1.a) and a picture of the experimental set-up (Fig. 1.b) with its specifications (Table 2) are shown. For more details of the experimental system, you can refer to Yamal et al. (2014).

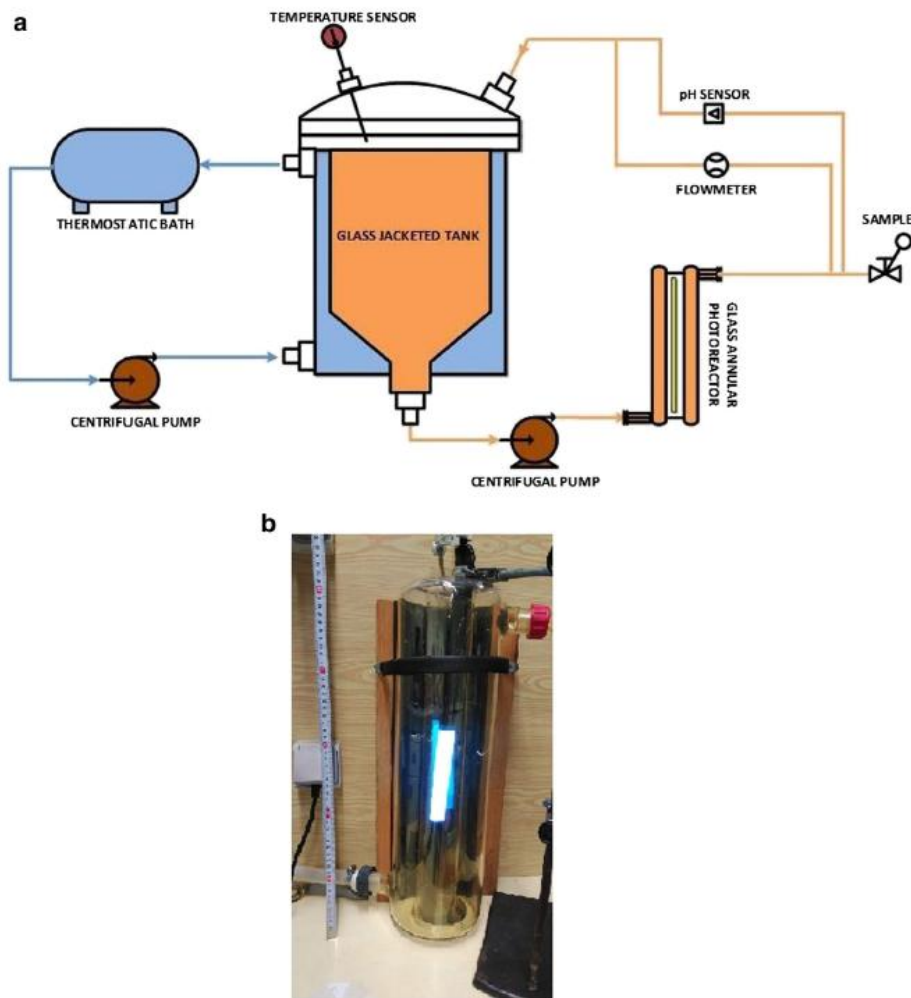


**Fig. 1.** Experimental set-up. **a)** Schematic view, **b)** Picture.



**Table 2.** Experimental device specifications

<b>TANK REACTOR</b>		
Total volume, L		<b>9</b>
<b>ANNULAR REACTOR</b>		
Total volume, L		<b>6</b>
Irradiated volume, L		<b>1.5</b>
Annular irradiated height, mm		<b>130</b>
Outer cylinder	Outer diameter, mm	<b>150</b>
	Inner diameter, mm	<b>140</b>
Inner cylinder	Outer diameter, mm	<b>70</b>
	Inner diameter, mm	<b>63.6</b>
<b>IRRADIATION SYSTEM</b>		
Actinic BL TL-DK 36 W/10 1SL		
Diameter, mm		<b>28</b>
Lenght, mm		<b>589.8</b>

#### 2.1.4 Experimental procedure

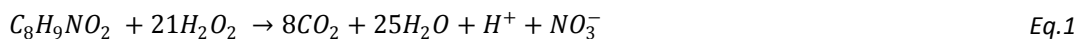
Fenton and photo-Fenton assays were performed in batch mode with recirculation, changing initial concentrations of hydrogen peroxide ( $C_{H_2O_2}^{t0}$ ) and ferrous ion ( $C_{Fe^{2+}}^{t0}$ ) for the same value of the initial concentration of PCT ( $C_{PCT}^{t0}$ ).

The value of the initial PCT concentration was set to 40 mg L<sup>-1</sup> in order to investigate Fenton and photo-Fenton treatment of a real paracetamol wastewater characterized by higher PCT concentrations (Dalgic et al. (2017)).

The maximum value of the initial concentration of Fe<sup>2+</sup> was set taking into account the maximum legal value in wastewaters in Spain (DOGC), 10 mg L<sup>-1</sup>, while half of such value was set as the minimum value to be investigated.

Also, to select the initial concentration of H<sub>2</sub>O<sub>2</sub>, the stoichiometric dose to achieve total mineralization when H<sub>2</sub>O<sub>2</sub> is considered to be the only oxidant in the media (Eq. 1) and when  $C_{PCT}^{t0} = 40$  mg L<sup>-1</sup>, was

calculated and resulted in a value of 189 mg L<sup>-1</sup>. Then, a range between half and twice the stoichiometric dose (94.5 and 378 mg L<sup>-1</sup>, respectively) was selected.



Eighteen experiments were carried out (Table 3) by testing three different values of  $C_{H_2O_2}^{t0}$  (94.5, 189, and 378 mg L<sup>-1</sup>) and  $C_{Fe^{2+}}^{t0}$  (5, 7.5, and 10 mg L<sup>-1</sup>), for the same value of  $C_{PCT}^{t0}$  set to 40 mg L<sup>-1</sup> (corresponding to  $C_{TOC}^{t0} = 25.40$  mg L<sup>-1</sup>) and under dark and irradiated conditions. Hence three hydrogen peroxide to paracetamol initial molar ratios (R=10.5, 21, 42) were investigated.

**Table 3.** Design of experiments.

ID	$C_{Fe^{2+}}^{t0}$ (mg L <sup>-1</sup> )	$C_{H_2O_2}^{t0}$ (mg L <sup>-1</sup> )	Irradiation	R (-)
				H <sub>2</sub> O <sub>2</sub> :PCT
E1	5	94.5	NO	10.5
E2	5	189	NO	21
E3	5	378	NO	42
E4	7.5	94.5	NO	10.5
E5	7.5	189	NO	21
E6	7.5	378	NO	42
E7	10	94.5	NO	10.5
E8	10	189	NO	21
E9	10	378	NO	42
E10	5	94.5	YES	10.5
E11	5	189	YES	21
E12	5	378	YES	42
E13	7.5	94.5	YES	10.5
E14	7.5	189	YES	21
E15	7.5	378	YES	42
E16	10	94.5	YES	10.5
E17	10	189	YES	21
E18	10	378	YES	42

Regarding the experimental protocol, the glass reservoir was first filled with 10 L of distilled water and then, after 15 min of recirculation, 4.9 L of distilled water in which PCT was previously dissolved, were added. Once pH was adjusted to  $2.8 \pm 0.1$ , the remaining 0.1L of distilled water, in which  $Fe^{2+}$  was previously dissolved, were filled and the light was switched on (in case of experiments performed under irradiated conditions). Finally,  $H_2O_2$  was added and the initial sample was taken. The total reaction time was fixed to 120 min. To ensure perfect mixing conditions, according to the results obtained by Yamal et al. (2014), the recirculation flow rate was set to  $12 \text{ L min}^{-1}$ .

## 2.2 MODELLING

The modelling section starts by proposing a kinetic model followed by the reactor model that allows describing, by the means of a set of ODEs, the mass balances into the photoreactor (isothermal conditions).

### 2.2.1 Kinetic model

The kinetic model proposed for the Fenton and photo-Fenton degradation of PCT (see *Table 4*) is based on the general Fenton/photo-Fenton reaction scheme proposed by Sun and Pignatello (1993a,b); Brillas et al.(2000); Pignatello et al.(2006).

**Table 4.** Reaction mechanism of Fenton and photo-Fenton PCT degradation

ID	Reaction steps	Kinetic constants
1	$Fe^{2+} + H_2O_2 \xrightarrow{k_1} Fe^{3+} + HO^- + HO^\cdot$	$k_1$
2	$Fe^{3+} + H_2O \xrightarrow{\overline{\Phi}} Fe^{2+} + H^+ + HO^\cdot$	$\overline{\Phi}$
3	$Fe^{3+} + H_2O_2 \xrightarrow{k_3} Fe^{2+} + H^+ + HO_2^\cdot$	$k_3$
4	$H_2O_2 + HO^\cdot \xrightarrow{k_4} HO_2^\cdot + H_2O$	$k_4$
5	$PCT + HO^\cdot \xrightarrow{k_5} P_i$	$k_5$

where  $\overline{\Phi}$  refers to the wavelength-averaged primary quantum yield that was taken from Bossman et al. (1998) and  $P_i$  represents the generic intermediate compound generated by the hydroxyl radical ( $HO^\cdot$ ) attack to PCT.

The proposed model is based on the following assumptions (Conte et al.2012):

- i. only the hydroxyl radicals ( $HO^\cdot$ ) are taken into account as oxidant species;
- ii. the steady-state approximation (SSA) can be applied to the highly reactive species ( $HO^\cdot$ );
- iii. low ferrous ion concentrations were selected so the hydroxyl radical attack to  $Fe^{2+}$  can be neglected;
- iv. the radical-radical termination steps are negligible compared to the propagation steps;
- v. the oxygen concentration is always in excess.

Hence, the kinetic constants accounting for Fenton and Fenton-like reactions, and the hydroxyl radical attack to hydrogen peroxide and paracetamol ( $k_1$ ,  $k_3$ ,  $k_4$ , and  $k_5$ , respectively) were the parameters to be estimated. Subsequently, the following reactions rates for the reactive species PCT,  $H_2O_2$ ,  $Fe^{2+}$  and  $Fe^{3+}$  were derived:

$$\begin{bmatrix} R_{PCT}(\underline{x}, t) \\ R_{H_2O_2}(\underline{x}, t) \\ R_{Fe^{2+}}(\underline{x}, t) \\ R_{Fe^{3+}}(\underline{x}, t) \end{bmatrix} = \begin{bmatrix} R_{PCT}^T(\underline{x}, t) \\ R_{H_2O_2}^T(\underline{x}, t) \\ R_{Fe^{2+}}^T(\underline{x}, t) \\ R_{Fe^{3+}}^T(\underline{x}, t) \end{bmatrix} + \overline{\Phi} \sum_{\lambda} e_{\lambda}^a(\underline{x}, t) \begin{bmatrix} -\frac{1}{\delta} \\ \frac{1}{\rho} \\ 1 \\ -1 \end{bmatrix} \quad Eq.2$$

Where

$$\delta = \frac{k_4}{k_{12}} \frac{C_{H_2O_2}}{C_{PCT}} + 1 \quad Eq.3$$

$$\rho = \frac{k_5}{k_4} \frac{C_{PCT}}{C_{H_2O_2}} + 1 \quad Eq.4$$

Here  $\overline{\Phi}$  is the wavelength-averaged primary quantum yield,  $\sum_{\lambda} e_{\lambda}^a(\underline{x}, t)$  the *LVRPA* extended to polychromatic radiation by performing the integration over all useful wavelengths  $\lambda$  (300-420 nm), and  $\underline{x}$  the position vector accounting for the radius and axial coordinates of the reactor.

It should be noted that the general reaction rate expression can be expressed as follows (in matrix notation):

$$[\mathbf{R}(\underline{x}, t)] = [\mathbf{R}^T(\underline{x}, t)] + \overline{\Phi} \sum_{\lambda} e_{\lambda}^a(\underline{x}, t) \boldsymbol{\tau}(\underline{x}, t) \quad Eq.5$$

The first term on the right-hand side of Eq.2 corresponds to the thermal reaction rate that gives the  $i$ -component degradation by the Fenton reaction, taking place in the total volume  $V_T$ , and is given by Eqs.6 and 7:

$$\begin{bmatrix} R_{PCT}^T(\underline{x}, t) \\ R_{H_2O_2}^T(\underline{x}, t) \\ R_{Fe^{2+}}^T(\underline{x}, t) \\ R_{Fe^{3+}}^T(\underline{x}, t) \end{bmatrix} = k_1 C_{Fe^{2+}} C_{H_2O_2} \begin{bmatrix} -\frac{1}{\delta} \\ -\left(1 + \frac{1}{\rho}\right) \\ -1 \\ +1 \end{bmatrix} + \gamma \begin{bmatrix} 0 \\ -1 \\ +1 \\ -1 \end{bmatrix} \quad Eq.6$$

where:

$$\gamma = k_2 C_{Fe^{3+}} C_{H_2O_2} \quad Eq.7$$

On the other hand, the second term on the right-hand side of Eq.2 corresponds to the  $i$ -component degradation by the radiation-activated reaction occurring inside the irradiated liquid volume ( $V_{IRR}$ ).

### 2.2.2 Reactor model

The mass balances and initial conditions for the well-stirred annular photoreactor are given by the following set of first order, ordinary differential equations:

$$\frac{d\mathbf{C}}{dt} = \mathbf{R}^T(t) + \frac{V_{IRR}}{V_T} \overline{\Phi} \left( \sum_{\lambda} e_{\lambda}^a(\underline{x}, t) \right)_{V_{IRR}} \boldsymbol{\tau}(\underline{x}, t) \quad Eq.8$$

With the initial conditions:

$$\mathbf{C} = \mathbf{C}^0 \quad t_0 = 0 \quad Eq.9$$

Note that the required reaction rate expressions to be replaced in Eq. 8 are given by Eqs. 2-4 and Eqs. 6-7.

Therefore, based on the previous considerations, the following ODEs system gives the mass balance equations of the reactor model for each species (PCT,  $H_2O_2$ ,  $Fe^{2+}$  and  $Fe^{3+}$ ):

$$\frac{dC_{PCT}}{dt} = \left[ \left( k_1 C_{Fe^{2+}} C_{H_2O_2} \left( -\frac{1}{\delta} \right) \right) \right] + \left[ \frac{V_{IRR}}{V_T} \left( \bar{\Phi} \left\langle \sum_{\lambda} e_{\lambda}^a(\underline{x}, t) \right\rangle_{V_{IRR}} \right) \right] \quad Eq.10$$

$$\frac{dC_{H_2O_2}}{dt} = \left[ \left( k_1 C_{Fe^{2+}} C_{H_2O_2} \left( -\left( 1 + \frac{1}{\rho} \right) \right) - \gamma \right) \right] + \left[ \frac{V_{IRR}}{V_T} \left( \bar{\Phi} \left\langle \sum_{\lambda} e_{\lambda}^a(\underline{x}, t) \right\rangle_{V_{IRR}} \right) \right] \quad Eq.11$$

$$\frac{dC_{Fe^{2+}}}{dt} = \left[ \left( -k_1 C_{Fe^{2+}} C_{H_2O_2} + \gamma \right) \right] + \left[ \frac{V_{IRR}}{V_T} \left( \bar{\Phi} \left\langle \sum_{\lambda} e_{\lambda}^a(\underline{x}, t) \right\rangle_{V_{IRR}} \right) \right] \quad Eq.12$$

$$\frac{dC_{Fe^{3+}}}{dt} = - \frac{dC_{Fe^{2+}}}{dt} \quad Eq.13$$

Here  $\langle \sum_{\lambda} e_{\lambda}^a(\underline{x}, t) \rangle_{V_{IRR}}$  is the LVRPA averaged over the irradiated reactor volume ( $V_{IRR}$ ). The latter depends on the spatial photon distribution within the annular photoreactor and, consequently, on the physical properties and the geometrical characteristics of the lamp-reactor system. To compute it, a radiation model must be previously introduced. Specifically, a line source model with spherical and isotropic emission (LSSE model) was adopted (Alfano et al. 1986; Braun et al. 2004). The LSSE model allows calculating  $LVRPA_{V_{IRR}}$  as a function of the radiation absorbing specie.

First, the following equation for the evaluation of the LVRPA for cylindrical coordinates has been solved using the numerical integration function in MATLAB:

$$e_{\lambda}^a(\underline{x}, t) = \kappa_{\lambda}(\underline{x}, t) \frac{P_{\lambda,s}}{2\pi L_L} \int_{\theta_1}^{\theta_2} \exp \left[ -\frac{\kappa_{T,\lambda}(\underline{x}, t)(r_i - r_{int})}{\cos \theta} \right] d\theta \quad Eq. 14$$

where  $P_{\lambda,s}$  is the lamp spectral power emission (provided by the lamp supplier),  $\kappa_{\lambda}(\underline{x}, t)$  the volumetric absorption coefficient of the reacting species,  $\kappa_{T,\lambda}(\underline{x}, t)$  the volumetric absorption coefficient of the medium,  $r$  the radius, and  $L_L$  the useful length of the lamp. To compute the radiation absorbed in a generic point  $I=l(r,z)$  (located at  $\underline{x}$ ) inside the reactor, it was necessary to estimate the limiting angles of integration (trigonometrically defined), that is:

$$\theta_1 = \tan^{-1} \left( \frac{r_i}{L_L - z_i} \right) \text{ and } \theta_2 = \tan^{-1} \left( \frac{-r_i}{z_i} \right) \quad Eq. 15$$

To solve Eq.14, it was considered that ferric ions present in solution as ferric ions complex ( $\text{Fe(OH)}^{2+}$ ) are the dominant ferric species at pH 2.8 and the principal absorbing specie; here it was also assumed that radiation absorption of hydrogen peroxide and ferrous ion is negligible for wavelengths greater than 300 nm. Under theses hypotheses,  $\kappa_{T,\lambda}(\underline{x}, t)$  can be calculated as follows:

$$\kappa_{T,\lambda}(\underline{x}, t) = \sum_i \alpha_{i,\lambda} C_i \cong \alpha_{\text{Fe(OH)}^{2+},\lambda} C_{\text{Fe(OH)}^{2+}} \quad \text{Eq. 16}$$

where  $\alpha_{\text{Fe(OH)}^{2+},\lambda}$  is the molar absorptivity of ferric ions complex ( $\text{Fe(OH)}^{2+}$ ) and  $C_{\text{Fe(OH)}^{2+}}$  is the concentration of the latter that can be considered equal to the concentration of  $\text{Fe}^{3+}$ .

Finally, after evaluating LVRPA at each point inside the irradiated volume, it is possible to compute the averaged value of the LVRPA over the irradiated reactor volume and polychromatic radiation, solving the following equation:

$$\langle \sum_{\lambda} e_{\lambda}^a(\underline{x}, t) \rangle_{V_{IRR}} = \frac{2\pi}{V_{IRR}} \int_0^L \int_{r_{int}}^{r_{ext}} e_{\lambda}^a(\underline{x}, t) r dr dz \quad \text{Eq. 17}$$

where  $r_{int}$  and  $r_{ext}$  are the internal and external radius of the annular photoreactor. Also in this case the numerical integration function in MATLAB was used to solve Eq.17.

In this way, it was possible to estimate the value of LVRPA averaged over the irradiated reactor volume for a specific set of values of  $C_{\text{Fe}^{3+}}$  (Table 5):

**Table 5.** Values of LVRPA averaged over the irradiated reactor volume, calculated for a specific set of iron concentration

$C_{\text{Fe}^{3+}} \text{ (mg L}^{-1}\text{)}$	$\langle \sum_{\lambda} e_{\lambda}^a(\underline{x}, t) \rangle_{V_{IRR}} \text{ (Einstein cm}^{-3} \text{ s}^{-1}\text{)}$
0.0	0
2.5	$3.5 \times 10^{-10}$
5.0	$7.1 \text{E} \times 10^{-10}$
7.5	$9.5 \times 10^{-10}$
10.0	$1.18 \times 10^{-9}$

## 2.3 MODEL FITTING AND PARAMETER ESTIMATION

A nonlinear multivariate and multiparameter optimization procedure was implemented in MATLAB in order to minimize the sum of the squared differences between the experimental and model values of PCT and  $\text{H}_2\text{O}_2$  normalized concentrations.

The first step is to solve numerically the ODEs system given by *Eqs.8* and *9*. For this purpose, an Ordinary Differential Equation (ODE) solver in MATLAB was used. Especially, ode15s solver stiff differential equations which is a variable-step, variable-order (VSVO) solver based on the numerical differentiation formulas (NDFs), was selected. Then, the values of the kinetic constants ( $k_1, k_3, k_4$  and  $k_5$ ) were estimated minimizing the sum of the squared differences between the model values (calculated by solving the ODEs system) and the experimental values of PCT and  $\text{H}_2\text{O}_2$ . For this purpose, the Levenberg-Marquardt least-squares algorithm available in the Optimization Toolbox of MATLAB was used. The whole set of experimental data (E1-E18, *Table 3*) was used for the parameter estimation. Additionally, the root mean square errors (*RMSE*) were calculated to test model reliability (see *Fig.2*).

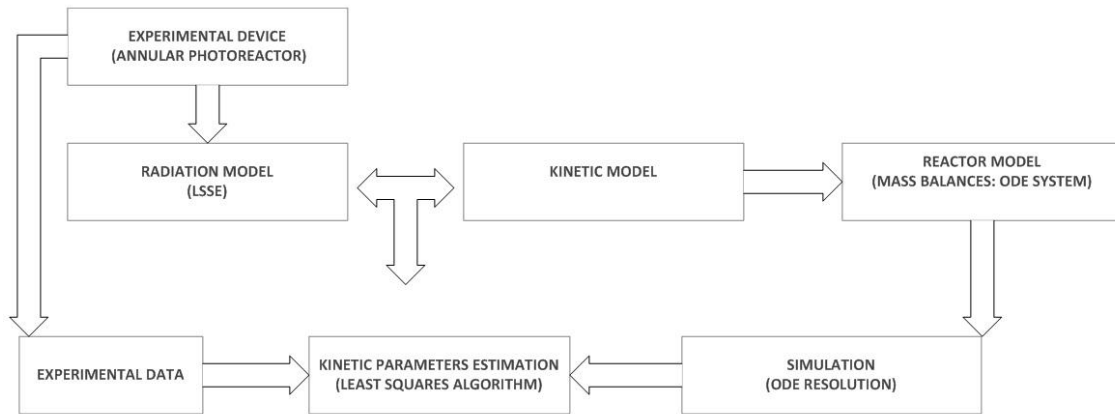


**Fig.2.** Flow diagram of the methodological framework followed to estimate the parameters of the proposed kinetic model

## 3 RESULTS AND DISCUSSION

### 3.1 EXPERIMENTAL RESULTS

Paracetamol was not detected by the HPLC analyses under all investigated conditions after a maximum time of 15 min (E1, *Table 3*) and a minimum time of 2.5 min (E18, *Table 3*) (results not shown).



Especially, for the highest value of  $C_{H_2O_2}^{t0}$ , and considering dark conditions and increasing  $C_{Fe^{2+}}^{t0}$  from 5, to 7.5 and 10 mg L<sup>-1</sup> (experiments E3, E6 and E9, *Table 3*), PCT total removal was obtained in 15, 10 and 5 min, respectively. In addition, for this dark conditions and considering the minimum concentration of oxidizing agent ( $C_{H_2O_2}^{t0} = 94.5 \text{ ppm}$ ), the reaction time necessary to achieve complete PCT destruction is reduced by 66% by doubling the initial catalyst concentration from 5 to 10 ppm (E1 and E7 tests respectively, *Table 3*). On the other hand, for the highest value of  $C_{H_2O_2}^{t0}$  and irradiating system (experiments E12, 15 and E18, *Table 3*), the PCT total conversion was obtained in only 10, 7.5 and 2.5 min, respectively. Therefore, considering irradiated conditions, by doubling the initial concentration of the catalyst, it is possible to reduce by up to 75% the time necessary for the complete destruction of the contaminant. Therefore, it was possible to confirm the beneficial effect of using higher doses of catalyst to reduce the reaction times necessary to achieve complete removal of the contaminant. This effect is of greater relevance for lower concentrations of oxidizing agent.

Although TOC was not introduced as a kinetic model component, it represents an important measurement to analyze the process performance. Hence, the performance of each experiment was also evaluated in terms of reached mineralization levels at a specific time (TOC conversion,  $X_{TOC}^{t,min}$ ). In *Fig. 3* the TOC experimental evolution obtained using the minimum (*Fig.3.a*) and maximum (*Fig.3.b*) concentrations of oxidizing agent and catalyst, is shown.

In *Fig.3a*, it can be observed that TOC conversion reaches asymptotic values in both experiments. Specifically,  $X_{TOC}^{75 \text{ min}} = 29.3\%$  and  $X_{TOC}^{60 \text{ min}} = 33\%$  for E1 and E10, respectively. However, these maximum conversion levels are associated with reaction times in which the oxidant agent is no more detected (75 and 60 min for E1 and E10, respectively). Although the TOC conversions obtained in both cases are similar, the use of radiation allowed reducing the reaction time by 20%. Therefore, even in the case of achieving the total removal of the contaminant (15 min of reaction) with the minimum concentrations of reagents, the level of mineralization reached is not significant. This is in accordance with the theoretical levels of oxidant agent doses required to achieve complete mineralization of the system (see *Eq.1*).

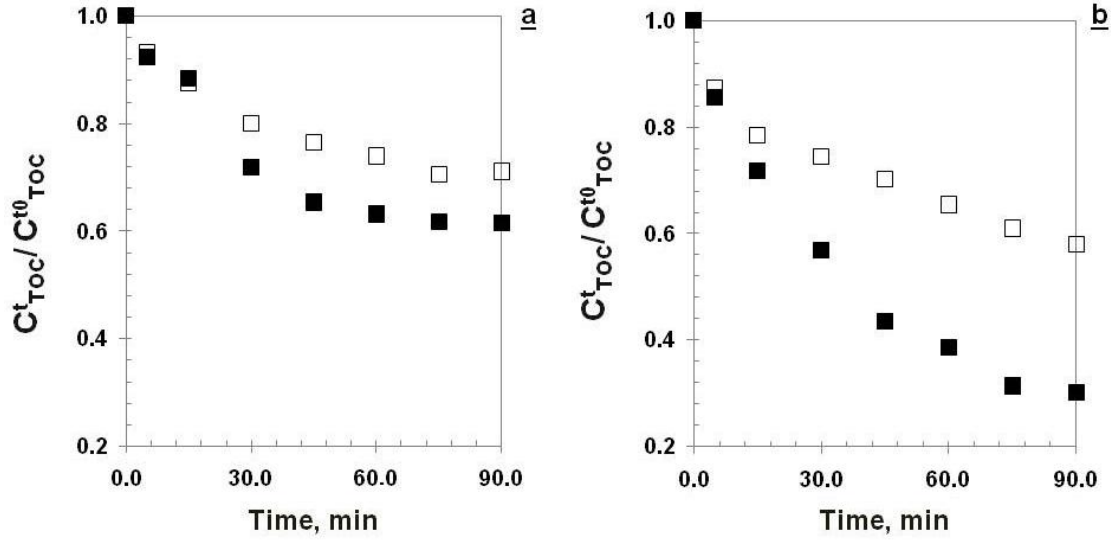


**Fig. 3.** Normalized experimental concentrations of TOC, obtained under dark ( $\square$ ) and irradiated ( $\blacksquare$ ) conditions and considering the lowest and highest initial concentrations of  $\text{Fe}^{2+}$  and  $\text{H}_2\text{O}_2$  ( $C_{\text{Fe}^{2+}}^{t0}$  and  $C_{\text{H}_2\text{O}_2}^{t0}$ ): experiments E1 and E10 **a)** and experiments E9 and E18 **b)**, respectively.

Furthermore, in Fig.3.b it can be appreciated an asymptotic value of  $X_{\text{TOC}}^{75 \text{ min}} = 68.5\%$  (depletion of  $\text{H}_2\text{O}_2$ ) in the case of the assay E18. This value was the highest level of mineralization that was reached for the whole set of performed experiments. Nevertheless, under the same maximum concentrations of the reagents, the dark reaction (E9), for which  $\text{H}_2\text{O}_2$  was detected until the end of the assay (120 min), only reached  $X_{\text{TOC}}^{120 \text{ min}} = 45.6\%$ .

Finally, in order to conclude the study regarding the mineralization performance of the system, the specific consumption of the oxidizing agent,  $\gamma_{\text{H}_2\text{O}_2/\text{TOC}}$ , was evaluated as follows:

$$\gamma_{\text{H}_2\text{O}_2/\text{TOC}} = \frac{C_{\text{H}_2\text{O}_2}^0 - C_{\text{H}_2\text{O}_2}^{t_f}}{C_{\text{TOC}}^0 - C_{\text{TOC}}^{t_f}} \quad \text{Eq. 18}$$

where  $t_f$  is the time at which the oxidizing agent consumption occurred or the final reaction time.

In Fig.4, a multiple bar chart shows the radiation effect on  $\gamma_{\text{H}_2\text{O}_2/\text{TOC}}$  obtained for several initial concentrations of the oxidant (94.5, 189 and 378  $\text{mg L}^{-1}$ ) and of the catalyst (5 and 10  $\text{mg L}^{-1}$ ).

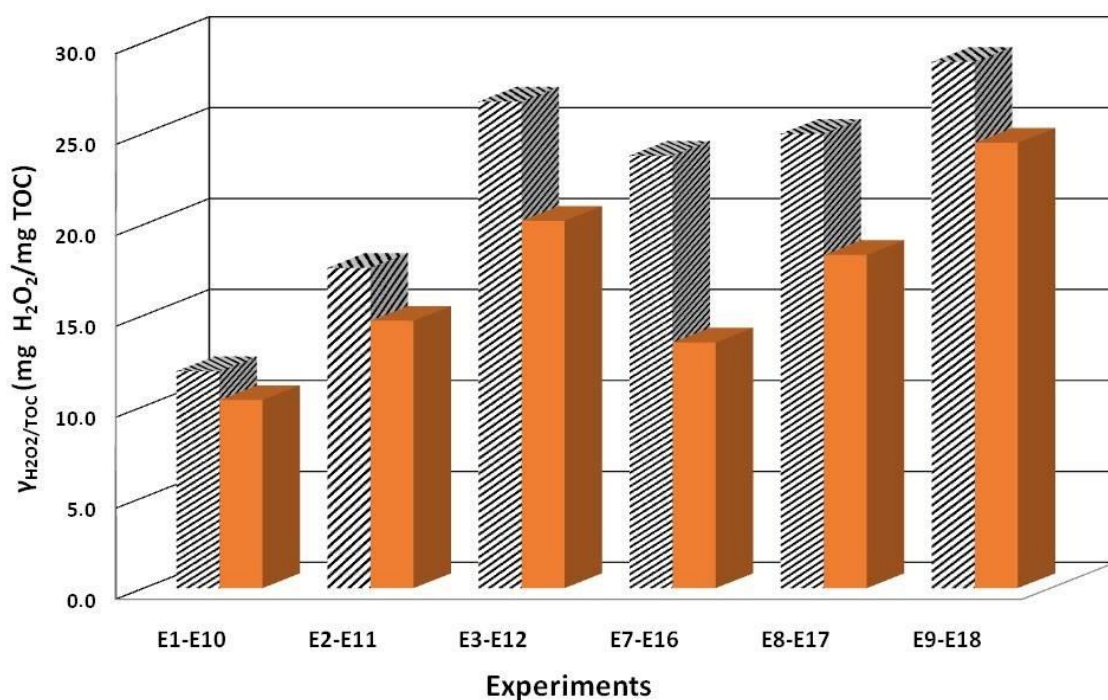


**Fig. 4.** Specific consumption of the oxidizing agent as a function of the experiments performed with  $C_{Fe^{2+}}^{to} = 5$  and  $10 \text{ mg L}^{-1}$  and for the three different investigated values of  $C_{H_2O_2}^{t0}$  ( $94.5, 189, 378 \text{ mg L}^{-1}$ ) under non irradiated (striped bar chart) and irradiated conditions (solid bar chart).

First of all, it must be noticed that for all the investigated conditions, the  $\mathcal{R}_{H_2O_2/TOC}$  results are always higher for non-irradiated conditions than for irradiated ones. This result highlights a less efficient consumption of  $H_2O_2$  under non-irradiated conditions. Moreover, it is possible to observe that the increase in the initial concentration of the catalyst led to an increase of the gap between the  $H_2O_2$  specific consumption obtained under non-irradiated and irradiated conditions.

It is worth noticed that, although the experiment E10 ( $C_{Fe^{2+}}^{to} = 5 \text{ mg L}^{-1}$  and  $C_{H_2O_2}^{t0} = 94.5 \text{ mg L}^{-1}$ ), carried out under irradiated conditions, showed to be the most efficient one, only allowed to reach a final TOC conversion of 39%. However, experiment E12 ( $C_{Fe^{2+}}^{to} = 5 \text{ mg L}^{-1}$  and  $C_{H_2O_2}^{t0} = 378 \text{ mg L}^{-1}$ ), also performed under irradiated conditions, despite being less efficient than E10, allowed to obtain a final TOC conversion of 74%. This result presents great environmental and economic significance since, according to the level of mineralization required by the system, it would allow knowing the dose of oxidizing agent

and necessary reaction time. Hence, this result shows that if, from one hand, the increase of the initial concentration of the oxidant led to a less efficient consumption of this last, from the other hand it allows reaching higher levels of mineralization.

### 3.2 MODEL FITTING

The experimental data were used to perform the fitting of the proposed kinetic model. The values of the kinetic parameters accounting for the Fenton and Fenton-like reactions ( $k_1$  and  $k_3$  respectively) and for hydroxyl radical attack to hydrogen peroxide and paracetamol ( $k_4$  and  $k_5$  respectively) were estimated and are shown in *Table 6*.

**Table 6.** Estimated values of the kinetic parameters

$k_1$	$k_3$	$k_4$	$k_5$
$\text{M}^{-1} \text{s}^{-1}$	$\text{M}^{-1} \text{s}^{-1}$	$\text{M}^{-1} \text{s}^{-1}$	$\text{M}^{-1} \text{s}^{-1}$
147.29	3.16	$7.00 \times 10^7$	$3.58 \times 10^9$

It is worth noting that the estimated values of the kinetic parameter  $k_4$  and  $k_5$  are within the range of values found in the specific literature (Simunovic et al. 2011, De Laurentiis et al. 2014). Conversely, the values of the kinetic parameters  $k_1$  and  $k_3$  result to be slightly higher than those found in the literature ( $63\text{-}76 \text{ M}^{-1} \text{s}^{-1}$  and  $0.01\text{-}0.02 \text{ M}^{-1} \text{s}^{-1}$ , respectively) (Simunovic et al. 2011).

In *Fig.5* the comparison between experimental and predicted concentrations of  $\text{H}_2\text{O}_2$  and PCT obtained for dark (*Fig. 5.a*) and irradiated conditions (*Fig. 5.b*), is shown.

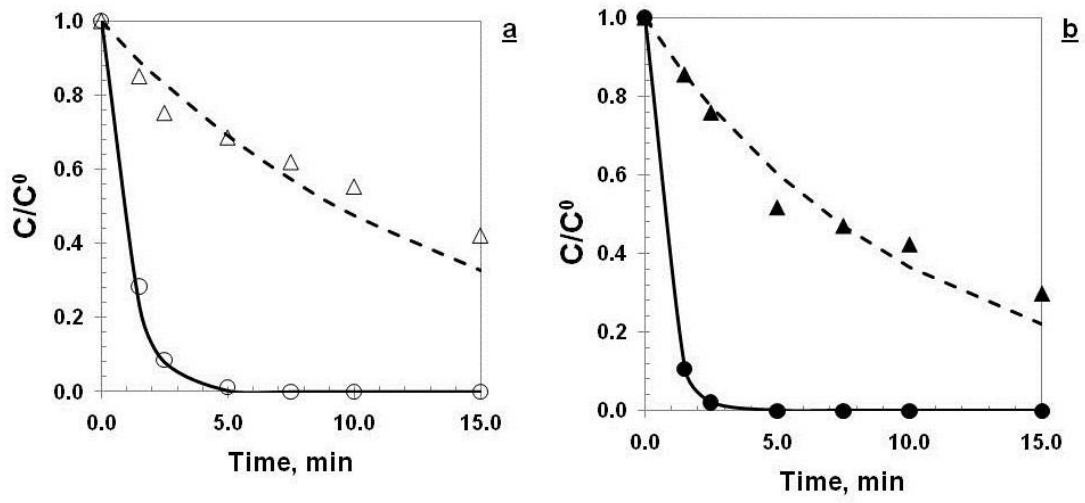


**Fig. 5.** Experimental concentrations of paracetamol ( $\circ, \bullet$ ) and hydrogen peroxide ( $\Delta, \blacktriangle$ ) and predicted concentrations of paracetamol ( $\text{—}$ ) and hydrogen peroxide ( $- -$ ). Dark ( $\circ, \Delta$ ) and irradiated ( $\bullet, \blacktriangle$ ) conditions. **a)** Experiment E6 ( $C_{Fe^{2+}}^{t_0} = 7.5 \text{ mg L}^{-1}$  and  $C_{H_2O_2}^{t_0} = 378 \text{ mg L}^{-1}$ ), and **b)** experiment E18 ( $C_{Fe^{2+}}^{t_0} = 10 \text{ mg L}^{-1}$  and  $C_{H_2O_2}^{t_0} = 378 \text{ mg L}^{-1}$ ).

Firstly, using the same initial concentration of  $H_2O_2$  under dark conditions and moving from  $C_{Fe^{2+}}^{t_0} = 7.5 \text{ mg L}^{-1}$  (Fig. 5.a) to  $C_{Fe^{2+}}^{t_0} = 10 \text{ mg L}^{-1}$  (data not shown), it was observed that the time at which PCT is no more detected by HPLC remained the same, approximately 5 min in both cases. However, it was observed that the irradiated condition (Fig. 5.b) led to the complete PCT removal in only 2.5 min. Hence, under these experimental conditions, the photo-Fenton process allowed to reach a 50% decrease in the total PCT removal time.

In order to test the model reliability, the root mean square error (*RMSE*) was calculated by the expression:

$$RMSE_i = \sqrt{\sum_k (y_{ik} - y_{ik}^*)^2 / n_i}, \quad \text{root mean square error of the } i^{th} \text{ variable} \quad \text{Eq.19}$$

$y_{ik}$ , value of the  $k^{th}$  measurement of the  $i^{th}$  variable

$y_{ik}^*$ , value of the  $k^{th}$  estimation of the  $i^{th}$  variable (model prediction)

$i = 1, 2, \dots, I$ ,  $i^{th}$  element of the set of measured variables

$k = 1, 2, \dots, n_i$ ,  $k^{th}$  element of the set of measurements of variable  $i$ ,

The only measurements considered are the normalized concentration of PCT and  $H_2O_2$  ( $I=2$ ).

In Table 7, the values of  $RMSE$ , calculated considering: i) the whole set of experiments (E1 to E18); ii) the experiments performed only under dark conditions (E1 to E9); and iii) the experiments performed only under irradiated conditions (E10 to E18), are shown.

**Table 7.** Root mean square errors ( $RMSE$ )

	<u>Dark and irradiated conditions</u>	<u>Dark conditions</u>	<u>Irradiated conditions</u>
<b>PCT</b>	6.80%	7.64%	5.84%
<b>H<sub>2</sub>O<sub>2</sub></b>	9.67%	9.75%	9.59%

The proposed model showed a relatively good agreement with the experimental data. The lowest values of  $RMSE$  (for normalized PCT and  $H_2O_2$  concentration) were obtained in case of considering only the experiments carried out under irradiated conditions. However, considering the complete set of performed tests, the obtained errors are consistent ( $RMSE_{PCT}=6.80\%$  and  $RMSE_{H_2O_2}=9.67\%$ ) and, therefore, the kinetic model is able to satisfactorily reproduce the system behaviour.

#### 4 CONCLUSIONS

The Fenton and photo-Fenton degradation of paracetamol and the consumption of hydrogen peroxide have been investigated in a well-stirred annular reactor placed inside the loop of a batch recycling system. Total removal of paracetamol was achieved for all the analysed operating conditions, with a maximum removal time of 15 min. Moreover, for each concentration of iron and oxidizing agent, no

significant differences were observed in the removal times required for both dark and irradiated tests. However, it should be mentioned that the reaction times were always lower for the irradiated operating conditions, with a minimum required time of 2.5 min.

In addition, the use of radiation allowed a significant enhancement of the process performance leading to a more efficient consumption of the oxidizing agent. For all the evaluated operating conditions, the values of the “specific consumption of the oxidant agent” ( $\chi_{H_2O_2/TOC}$ ) obtained for Fenton process were always higher than the corresponding values observed for photo-Fenton system.

Furthermore, the performance of each experiment was also evaluated in terms of reached mineralization levels at a specific reaction time. The highest level of mineralization achieved considering the whole set of experiments was  $X_{TOC}^{75min} = 68.5\%$ , conversion value obtained at the time when the oxidizing agent had been completely consumed.

A kinetic model for predicting Fenton and photo-Fenton degradation of paracetamol and hydrogen peroxide consumption has been proposed. Results have shown that the proposed kinetic model is able to capture the complex and nonlinear nature of such processes and incorporate the effect of the Local Volumetric Rate of Photon Absorption on the reactor behaviour.

Kinetic parameters, accounting for the Fenton and photo-Fenton reaction and the  $HO^\bullet$  attack to PCT and  $H_2O_2$  were estimated. Considering the values of the root mean square error ( $RMSE$ ) obtained for the complete set of experimental runs ( $RMSE_{PCT}=6.80\%$  and  $RMSE_{H_2O_2}=9.67\%$ ), it was possible to conclude that the proposed kinetic model is able to satisfactorily reproduce the system behaviour.

This kinetic model is the starting point for the development of a more complex model that also takes into account the generation of intermediate compounds and the evolution of the total organic carbon, and their main effects on the reaction rate of the photo-Fenton system.

## ACKNOWLEDGEMENTS

Financial support received from the Spanish "Ministerio de Economía, Industria y Competitividad" and the European Regional Development Fund, both funding the research Project AIMS (DPI2017-87435-R) is fully acknowledged.

Also, the authors acknowledge the financial support from the Universidad Nacional del Litoral (UNL, Project PIC50420150100009LI), Consejo Nacional de Investigaciones Científicas y Técnicas (CONICET, Project PIP-2015 0100093), and Agencia Nacional de Promoción Científica y Tecnológica of Argentina (ANPCyT, Project PICT-2015-2651). Francesca Audino, particularly acknowledges the MINECO for the PhD grant (BES-2013-065545).

## REFERENCES

Alfano OM, Romero RL, Cassano AE (1986) Radiation field modelling in photoreactors-I. Homogeneous media. Chemical Engineering Science 41(3): 421-444

Andreozi R, Caprio V, Insola A, Marotta R (1999) Advanced oxidation processes (AOP) for water purification and recovery. Catalysis Today 53(1): 51-59

Andreozi R, D'Apuzzo A, Marotta R (2000) A kinetic model for the degradation of benzothiazole by Fe<sup>3+</sup>-photo-assisted Fenton process in a completely mixed batch reactor. Journal of Hazardous Material B 80(1-3): 241-257

Antunes SC, Freitas R, Figueira E, Gonçalves F, Nunes B (2013) Biochemical effects of acetaminophen in aquatic species: edible clams *Venerupis decussata* and *Venerupis philippinarum*. Environmental Science and Pollution Research 20(9): 6658-6666

Bossmann SH, Oliveros E, Göb S, Siegwart S, Dahlen EP, Payawan Jr L, Straub M, Wörner M, Braun AM (1998) New evidence against hydroxyl radicals as reactive intermediates in the thermal and photochemically enhanced Fenton reactions. Journal of Physical Chemistry A 102(28): 5542–5550

Braun AM, Jacob L, Oliveros E, Oller do Nascimento CA (2004) Up-scaling photochemical reactions. Advances in Photochemistry 18: 235-313



Brillas E, Calpe JC, Casado J (2000) Mineralization of 2,4-D by advanced electrochemical oxidation processes. *Water Research* 34(8):2253-2262

Cabrera Reina A, Santos-Juanes L, García JL, Casas JL, Sánchez JS (2012) Modelling photo-Fenton process for organic matter mineralization, hydrogen peroxide consumption and dissolved oxygen evolution. *Applied Catalysis B: Environmental* 119-120: 132-138

Cassano AE, Martin CA, Brandi RJ, Alfano OM (1995) Photoreactor Analysis and Design: Fundamentals and Applications. *Industrial & Engineering Chemistry Research* 34(7): 2155-2201

Conte LO, Farias J, Albizzati ED, Alfano OM (2012) Photo-Fenton Degradation of the Herbicide 2,4-Dichlorophenoxyacetic Acid in Laboratory and Solar Pilot-Plant Reactors. *Industrial & Engineering Chemistry Research* 51(11): 4181–4191

Conte LO, Schenone AV, Alfano OM (2016) Photo-Fenton degradation of the herbicide 2,4-D in aqueous medium at pH conditions close to neutrality. *Journal of Environmental Management* 170: 60-39

Dalgic G, Turkdogan IF, Yetilmezsoy K, Kocak E (2017) Treatment of real paracetamol wastewater by Fenton process. *Chemical Industry & Chemical Engineering Quarterly* 23(2): 177–186

De Gusseme B, Vanhaecke L, Verstraete W, Boon N (2011) Degradation of acetaminophen by *Delftia suruhatensis* and *Pseudomonas aeruginosa* in a membrane bioreactor. *Water Research* 45(4): 1829-1837

De Laurentiis E, Prasse C, Ternes TA, Minella M, Maurino V, Minero C, Sarakha M, Brigante M, Vione D (2014) Assessing the photochemical transformation pathways of acetaminophen relevant to surface waters: Transformation kinetics, intermediates, and modeling. *Water Research* 53: 235-248

DOGC núm. 3894, DECRET 130/2003, de 13/05/2003, (29.5.2003). (URL: <http://www.gencat.cat/diari/3894/03127147.htm>, accessed 15/09/2017)

Fenton HJH (1894) Oxidation of tartaric acid in the presence of iron. *Journal of the Chemical Society* 65: 899-910

Farias J, Rossetti GH, Albizzati ED, Alfano OM (2007) Solar Degradation of Formic Acid: Temperature Effects on the Photo-Fenton Reaction. *Industrial & Engineering Chemistry Research* 46(23): 7580-7586

GöbS, Oliveros E, Bossmann SH, Braun AM, Nascimento CA, Guardani R (2001) Optimal experimental design and artificial neural networks applied to the photochemically enhanced Fenton reaction. *Water Science and Technology: a Journal of the International Association on Water Pollution Research* 44(5):339-345

ISO 6332:1988. Water quality — Determination of iron — Spectrometric method using 1, 10-phenanthroline

Jeyong J, Yoon J (2005) pH effect on OH radical production in photo/ferrioxalate system. *Water Research* 39(13): 2893–2900

Kang N, Dong SL, Jeyong Y (2002) Kinetic modeling of Fenton oxidation of phenol and monochlorophenols. *Chemosphere* 47(9): 915–924

Kiwi J, Pulgarin C, Peringer P, Gratzel M (1993) Beneficial effect of homogeneous photo-Fenton pretreatment upon the biodegradation of anthraquinonesulfonate in wastewater treatment. *Applied Catalysis B: Environmental* (3): 85-99

Kusic H, Koprivanac N, Loncaric A, Selanec I (2006) Photo-assisted Fenton type processes for the degradation of phenol: a kinetic study. *Journal of Hazardous Materials* 136(3): 632–644

Langford KH, Thomas KV (2009) Determination of pharmaceutical compounds in hospital effluents and their contribution to wastewater treatment works. *Environmental International* 35(5): 766–770

Miralles-Cuevas S, Audino F, Oller I, Sánchez-Moreno R, Sánchez Pérez JA, Malato S (2014) Pharmaceuticals removal from natural water by nanofiltration combined with advanced tertiary treatments (solar photo-Fenton, photo-Fenton-like Fe(III)–EDDS complex and ozonation). *Separation and Purification Technology* 122: 515–522

Muir N, Nichols J, Stillings M, Sykes J (1997) Comparative bioavailability of aspirin and Paracetamol following single dose administration of soluble and plain tablets. *Current Medical Research and Opinion* 13(9): 491–500

Murov SL, Carmichael I, Hug GL (1993) *Handbook of photochemistry*. 2nd ed., Dekker, New York

Nogueira RFP, Oliveira MC, Paterlini WC (2005) Simple and fast spectrophotometric determination of H<sub>2</sub>O<sub>2</sub> in photo-Fenton reactions using metavanadate. *Talanta* 66(1):86–91

Oller I, Malato S, Sánchez-Pérez JA (2011) Combination of Advanced Oxidation Processes and biological treatments for wastewater decontamination—A review. *Science of the Total Environment* 409(20): 4141–4166

Ortiz de la Plata GB, Alfano OM, Cassano AE (2010) Decomposition of 2-chlorophenol employing goethite as Fenton catalyst. I. Proposal of a feasible, combined reaction scheme of heterogeneous and homogeneous reactions. *Applied Catalysis B: Environmental* 95(1-2): 1-13

Pérez-Moya M, Graells M, Buenestado P, Mansilla HD (2008) A comparative study on the empirical modeling of photo-Fenton treatment process performance. *Applied Catalysis B: Environmental* 84(1-2): 313–323

Pignatello J, Oliveros E, MacKay A (2006) Advanced oxidation processes for organic contaminant destruction based on the Fenton reaction and related chemistry. *Critical Reviews in Environmental Science and Technology* 36(1):1–84

Pouran SR, Aziz ARA, Mohd W, Wan A (2015) Review on the main advances in photo-Fenton oxidation system for recalcitrant wastewaters. *Journal of Industrial and Engineering Chemistry* 21: 53-69

Pulgarin C, Kiwi J (1996) Overview on photocatalytic and electrocatalytic pretreatment of industrial non-biodegradable pollutants and pesticides. *CHIMIA International Journal for Chemistry* 50(3): 50-55

Ribeiro AR, Nunes OC, Pereira MFR, Silva AMT (2015) An overview on the advanced oxidation processes applied for the treatment of water pollutants defined in the recently launched Directive 2013/39/EU. *Environment International* 75: 33–51

Roshanfekar L, Irani M, Divsar F, Pourahmad H, Sadegh Sayyafan M, Haririan I (2015) Simultaneous degradation of phenol and paracetamol during photo-Fenton process: Design and optimization. *Journal of the Taiwan Institute of Chemical Engineers* 47:190-196

Shokry A, Audino F, Vicente P, Escudero G, Graells M, Pérez-Moya M, Espuña A, Proceedings of 12th PSE and 25th ESCAPE Joint Event, Copenhagen, Denmark, 2015

Simunovic M, Kusic H, Koprivanac N, Loncaric Bozic A (2011) Treatment of simulated industrial wastewater by photo-Fenton process: Part II. The development of mechanistic model. *Chemical Engineering Journal*, 173(2): 280– 289

Sun Y, Pignatello JJ (1993a) Photochemical reactions in the total mineralization of 2,4-D by Fe<sup>3+</sup>/H<sub>2</sub>O<sub>2</sub>/UV. *Environmental Science and Technology* 27(2): 304-310

Sun Y, Pignatello JJ (1993b) Organic intermediates in the degradation of 2,4-dichlorophenoxyacetic acid by  $\text{Fe}^{3+}/\text{H}_2\text{O}_2$  and  $\text{Fe}^{3+}/\text{H}_2\text{O}_2/\text{UV}$ . *Journal of Agricultural and Food Chemistry* 41(7): 1139-1142

Ternes TA (1998) Occurrence of drugs in German sewage treatment plants and rivers. *Water Research* 32(11): 3245–3260

United States Environmental Protection Agency (EPA). <https://www.epa.gov/wqc/contaminants-emerging-concern-including-pharmaceuticals-and-personal-care-products>

Wang N, Zheng T, Zhang G, Wang P (2016) A review on Fenton-like processes for organic wastewater treatment. *Journal of Environmental Chemical Engineering* 4(1): 762–787

Yamal-Turbay OE, Conte LO, Graells M, Mansilla HD, Alfano OM, Pérez-Moya M (2014) Photonic efficiency of the photodegradation of Paracetamol in water by the photo-Fenton process. *Environ Science and Pollution Research* 22(2): 938-945

Zapata A, Oller I, Rizzo L, Hilgert S, Maldonado MI, Sánchez-Pérez JA, Malato S (2010) Evaluation of operating parameters involved in solar photo-Fenton treatment of wastewater: Interdependence of initial pollutant concentration, temperature and iron concentration. *Applied Catalysis B* 97(1-2): 292–298